Chemical Engineering Journal 359 (2019) 186–196

Contents lists available at ScienceDirect

Chemical Engineering Journal

journal homepage: www.elsevier.com/locate/cej

Rational design of graphic carbon nitride copolymers by molecular doping for visible-light-driven degradation of aqueous sulfamethazine and hydrogen evolution

Chengyun Zhou[a,1], Piao Xu[a,1], Cui Lai[a,1], Chen Zhang[a,1], Guangming Zeng[a,*], Danlian Huang[a,*], Min Cheng[a], Liang Hu[a], Weiping Xiong[a], Xiaofeng Wen[a], Lei Qin[a], Jili Yuan[b], Wenjun Wang[a]

[a] College of Environmental Science and Engineering, Hunan University and Key Ministry of Education, 8 South Lushan Road, Yuelu District, Changsha 410082, PR China
[b] College of Materials Science and Engineering, Hunan University, 8 South Lushan Road, Yuelu District, Changsha 410082, PR China

HIGHLIGHTS

- TCN was prepared by molecular copolymerization of urea and 2-thiobarbituric acid.
- The band gap of TCN could be adjusted by changing the amount of 2-thiobarbituric acid.
- TCN exhibited enhanced photocatalytic activity for hydrogen production and SMZ degradation.
- Enhanced charge carrier separation efficiency is obtained by modification.

GRAPHICAL ABSTRACT

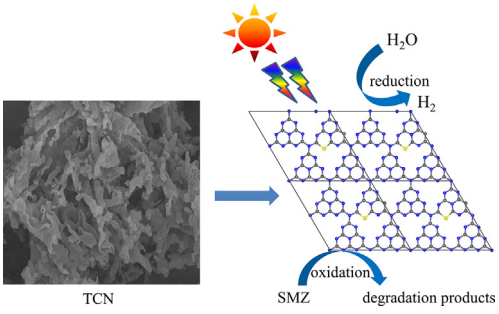

ARTICLE INFO

Keywords:
Carbon nitride
Molecular doping copolymerization
Charge carriers transfer
Photocatalytic hydrogen evolution
Photocatalytic degradation

ABSTRACT

Carbon nitride is a promising metal-free visible light driven photocatalyst and sustainable material for address contaminant pollution and water splitting. However, the insufficient visible light absorption and fast charge recombination of carbon nitride have limited its practical application. Herein, the self-assembly carbon nitride (denoted as TCN) by molecular doping copolymerization of urea and 2-thiobarbituric acid (TA) was prepared. XPS and elemental analytical results indicated that TA was doped in the framework of carbon nitride successfully. The self-assembly copolymerization would result in the change of morphology, intrinsic electron and band structure of carbon nitride. Theoretical calculations and experiments confirm that the band gap of TCN could be adjusted by changing the amount of 2-thiobarbituric acid. Moreover, the efficiency of charge carrier transfer and separation was greatly enhanced. As a result, the optimized photocatalyst TCN-0.03 exhibited superior activity with a high reaction rate of 0.058 min^{-1} for the degradation of sulfamethazine under visible light irradiation, which is 4.2 times higher than that of urea based carbon nitride (U-CN). As a multifunctional photocatalyst, TCN-0.03 showed enhanced activity for hydrogen production (55 μmol h^{-1}), which was 11 times higher than U-CN. The apparent quantum efficiency reached to 4.8% at 420 nm. A possible mechanism was proposed to explain the photocatalytic reaction process. This work provides insight into the rational design of modified carbon nitride by other organic monomers copolymerization to enhance the photocatalytic activity.

* Corresponding authors at: College of Environmental Science and Engineering, Hunan University, Changsha, Hunan 410082, PR China.
E-mail addresses: zgming@hnu.edu.cn (G. Zeng), huangdanlian@hnu.edu.cn (D. Huang).
[1] These authors contribute equally to this article.

https://doi.org/10.1016/j.cej.2018.11.140
Received 20 September 2018; Received in revised form 13 November 2018; Accepted 18 November 2018
Available online 19 November 2018
1385-8947/

1. Introduction

Due to the rapid development of economy, a series of worldwide problems such as energy shortage crisis appeared [1–6]. Hydrogen is considered as one of the most important clean fuels in the future. Photocatalytic hydrogen production has received great attention since it offers an ideal solution for energy shortage by using water and light. On the other hand, water pollution has become a global issue in recent decades, especially the persistent organic pollutants in natural water environment [7–10]. These pollutants may pose risks to human health even at a low concentration and are difficult to be removed by traditional treatments [11–16]. Semiconductor photocatalysis is a promising method for environmental remediation and clean energy generation [17–22]. Under light illumination, photogenerated electrons and holes are generated and transferred to the semiconductor surface, where they react with the molecular oxygen and hydroxyls to produce reactive oxygen species (ROS, typically including ·OH, $\cdot O_2^-$, and H_2O_2) and then mineralize pollutants [23–29]. Therefore, it is particularly important to develop sustainable and efficient photocatalysts.

As a metal free organic polymer semiconductor, graphitic carbon nitride (g-C_3N_4) has triggered considerable interest because of its superior chemical stability and simple preparation method in the last decades [30–34]. The band gap (about 2.7 eV) and band edge position (about 460 nm) of carbon nitride are suitable for various applications, such as water splitting, contaminant degradation, organic synthesis, CO_2 conversion and H_2O_2 production under visible light illumination [35–37]. However, many carbon nitrides were synthesis by simply calcination of melamine, urea, or thiourea. Practical applications of carbon nitride are limited for the fast charge carriers recombination, low surface area and limited light absorption. To obtain sufficient solar-to-energy conversion efficiency, it is reasonable to optimize the structural, textural and electronic properties of the carbon nitride [38]. Several methods have been made to improve photocatalytic activity of g-C_3N_4, such as element doping [39–41], and heterojunction with other semiconductors [42]. Additionally, copolymerization has been applied to improve the light absorption and enhance the efficiency separation of charge carriers [43–45].

Conjugated organic polymers present some advantages including sustainable, cost effective, and tunable band gap, which can be adjusted by various organic compounds [46,47]. Supramolecular assembly copolymerization of different precursors has become an attractive method to enhance the activities and properties of g-C_3N_4 [48,49]. In our previous studies, g-C_3N_4 photocatalyst was prepared using melamine and other organic monomers by copolymerization, which exhibited highly enhanced photocatalytic activity for antibiotics degradation [24,50,51]. Compared with melamine and dicyandiamide, the g-C_3N_4 prepared by urea showed better photocatalytic activity due to the higher polymerization degree and larger surface area. For example, Qiu et al. synthesized oxygen doped g-C_3N_4 by self-assembly polymerization of urea and oxalic acid, which showed extensive visible light absorption and well degradation efficiency of bisphenol A (BPA) [52]. Recently, Zhang et al. reported a g-C_3N_4 nanotube by condensation of urea and oxamide, which exhibited increased H_2 evolution activities under green light illumination [53,54]. Therefore, it is desirable to design the modification of g-C_3N_4 in the structure and localized electronic distribution, which may be beneficial to advance the light absorption and the charge separation.

In this work, 2-thiobarbitucid acid (TA) as a urea similar structure could be incorporated into the classical carbon nitride structure. The newly carbon nitride was prepared by mixing urea with different amount of TA, and then heated at 550 °C to induce copolymerization. The resulting product was denoted as TCN-x, where x was represented the amount of TA. The two monomers could form a cross-linked complex by hydrogen bond and generate unique carbon nitride. The photocatalytic activity was tested by measuring the degradation of sulfamethazine and hydrogen evolution under visible light illumination. The optical properties of prepared samples were characterized by theoretical calculations and experiments. The main radicals in the photodegradation system were studied by radicals trapping experiment and electron spin-resonance spectroscopy (ESR) analysis. This work provides insight into the rational design of modified carbon nitride with other organic monomers copolymerization to enhance the photocatalytic activity.

2. Experimental

2.1. Materials

Urea (> 99%), 2-thiobarbituric acid (> 99%), and sulfamethazine (> 99%) were purchased from Sinopharm Chemical Reagent Co., Ltd (Shanghai, China). All the reagents and materials are of analytical grade and used as received without additional purification or treatment. De-ionized water (18.25 MΩ.cm) was used in the whole experiment.

2.1.1. Synthesis of urea based carbon nitride (U-CN)

The typical bulk carbon nitride was prepared by a traditional polymerization as reported previously [53,55]. In a typical procedure, 10 g of urea was placed in a ceramic crucible with a cover and heated at 3.6 °C min^{-1} to 550 °C and maintained for 2 h in air. After cooling to ambient temperature, the reacted mass was washed repeatedly with distilled water. The resultant product was dried at 80 °C and labeled as U-CN.

2.1.2. Synthesis of TCN samples

The TCN samples were prepared from urea, 2-thiobarbituric acid (TA) by a facile wet chemistry method and thermal treatment. Typically, 10 g of urea and a known amount of 2-thiobarbituric acid (0.01 g, 0.03 g, 0.05 g, and 0.1 g) were mixed with 5 mL of de-ionized water and 5 mL ethanol to form the hydrogen bond interaction. The above mixed solution was dried at 90 °C. The obtained dried products were placed in a ceramic crucible with a cover and heated at 3.6 °C min^{-1} to 550 °C and maintained for 2 h in air. After cooling to ambient temperature, the reacted mass was washed repeatedly with de-ionized water. The resultant product was dried at 80 °C in vacuum. The product labeled as TCN-x, where x represents the amount of TA (x = 0.01, 0.03, 0.05, and 0.1 g, respectively) for simplify.

2.2. Characterization methods

The X-ray diffraction (XRD) patterns were achieved from a Rigaku D/max-2500 instrument with Cu Kα radiation (λ = 0.15406 nm) and Fourier transform infrared spectroscopy (FTIR) spectra were obtained by BIO RAD FTS-600 spectrometer. The morphologies of photocatalysts were examined on FEI Helios NanoLab 600i scanning electron microscopy (SEM) and FEI tecnai G2F20 transmission electron microscopy (TEM). The X-ray photoelectron spectra (XPS) of samples were investigated on ESCALAB 250Xi spectrometer. The UV–vis diffuse reflectance spectra (DRS) of samples were measured on a Cary 300UV–vis spectrophotometer with $BaSO_4$. Room temperature photoluminescence (PL) spectra were obtained at a Perkin Elmer luminescence spectrometer (LS 50B) with excitation wavelength of 365 nm. Average fluorescent lifetime was calculated as follows: $\tau_A = (A_1\tau_1^2 + A_2\tau_2^2)/(A_1\tau_1 + A_2\tau_2)$.

2.3. Photocatalytic degradation of pollutants

The photocatalytic degradation of pollutants by all samples was performed under visible light irradiation from a 300 W Xenon lamp with a 420 nm filter. In a typical test, 50 mg of powder photocatalyst was dispersed into 50 mL of sulfamethazine (SMZ, 10 mg L^{-1}) solution and stirred in dark to reach the adsorption-desorption equilibrium. At a given time interval of irradiation, 2 mL suspension was taken from the

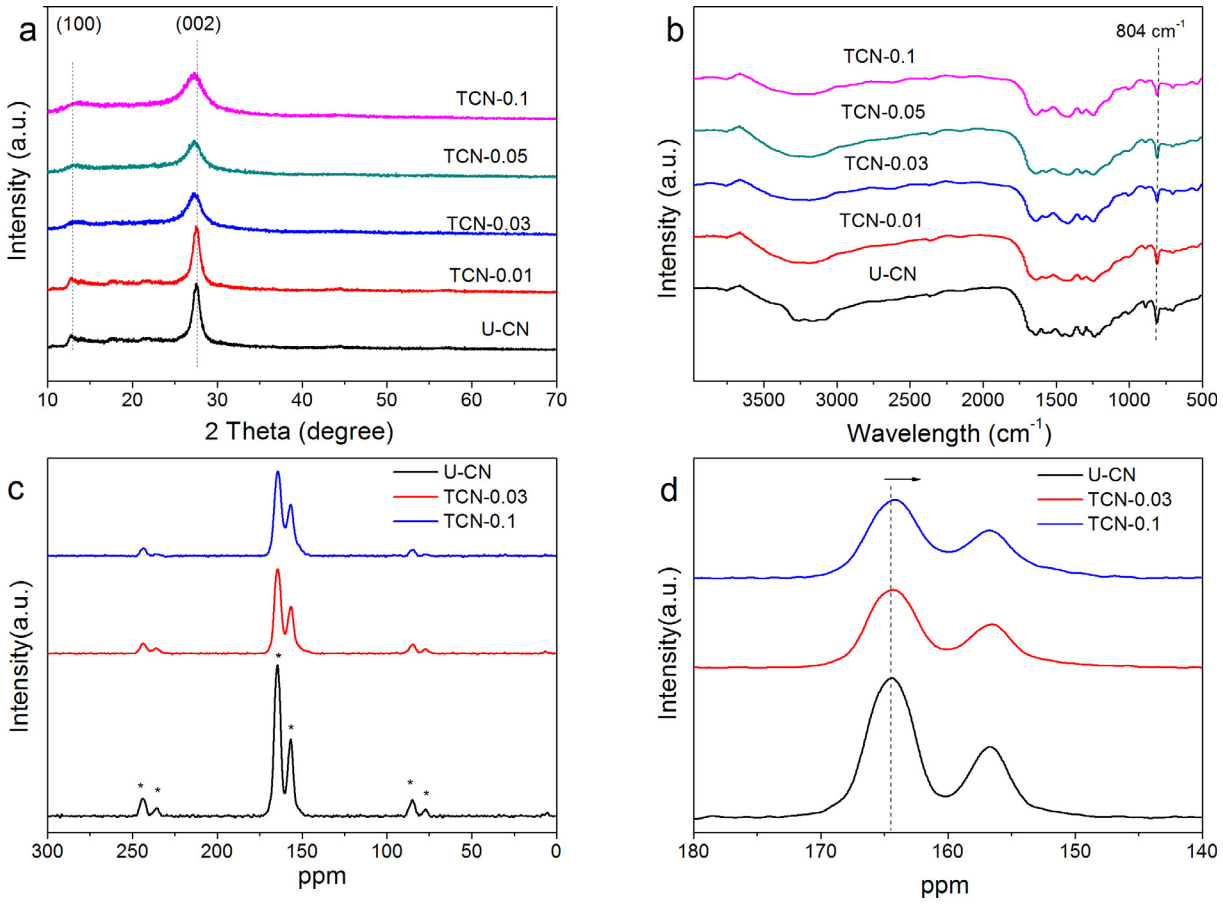

Fig. 1. (a) XRD patterns and (b) FT-IR spectra of U-CN and TCN samples; (c, d) Solid-state ^{13}C NMR spectra of U-CN, TCN-0.03 and TCN-0.1.

reactor and centrifuged. The SMZ concentration was determined using an HPLC Series 1100 (Agilent, Waldbronn, Germany) equipped with a UV–vis detector. The Column was C-18 column (4.6 × 250 mm) at the temperature of 30 °C. The HPLC analysis method for SMZ was based on the previous study and had a mobile phase of 80:20 0.02 M acetic acid: methanol, a flow rate of 1 mL min^{-1}, an injection volume of 20 μL, and a 270 nm detection wavelength [56].

2.4. Photocatalytic hydrogen evolution

Photocatalytic hydrogen evolution was carried out in a Pyrex top-irradiation vessel connected to a closed gas circulation and evacuation (Labsolar-6A). 50 mg of catalyst was dispersed in 100 mL of aqueous solution containing 10 vol% triethanolamine as electron sacrificial agent. 3 wt% Pt co-catalysts were deposited by an in-situ photo-deposition strategy from H_2PtCl_6 precursor. The solution was irradiated by a 300 W xenon arc lamp equipped with a 420 nm cut-off filter. The evolved gases were analyzed in-situ by a Fuli GC9790II gas chromatography equipped with a thermal conductive detector (TCD) and a 5 Å molecular sieve column, using Argon as the carrier gas. The apparent quantum yield (AQY) for hydrogen production was measured using the wavelength of 420, 450, 500 and 520 nm band-pass filters. The AQY was calculated by the following equation: AQY = number of evolved H_2 molecules × 2 × 100/number of incident photons.

2.5. Photoelectrochemical measurement

Photoelectrochemical tests were carried out on a CHI 660D workstation in a three-electrode cell, using a Pt electrode (40 × 0.55 mm, 99%) as the counter electrode and an Ag/AgCl electrode as the reference electrode. The working electrodes were prepared on F-doped tin oxide (FTO) glass, which was cleaned by ethanol and dried at 80 °C. The 5 mg of the photocatalyst was suspended in 1 mL of 0.5% nafion solution to get a slurry mixture. Then, 100 μL of the slurry dropped onto a 1 cm × 2 cm FTO slice with an effective working area of 1 cm^2. After air-drying, the working electrode was further dried at 120 °C for 2 h to improve adhesion. A 300 W Xenon lamp was used as a light source. The electrochemical impedance spectroscopy (EIS) was performed in 100 mL of 0.2 M Na_2SO_4 aqueous solution with the above three-electrode system.

2.6. Calculation method

To understand the role of incorporated TA into the CN framework, the density functional theory (DFT) were carried out by using the Vienna Ab-initio Simulation Package (VASP) package. The electronic properties and band gap were calculated by employing the Heyd-Scuseria-Ernzerh of hybrid functional (HSE06) method. The U-CN and TCN in which part of nitrogen was substituted with carbon and sulfur were employed for the DFT calculation. Uniform G-centered k-points meshes with a resolution of $2\pi * 0.03\ Å^{-1}$ and Methfessel-Paxton electronic smearing were adopted for the integration in the Brillouin zone for geometric optimization. The simulation was run with a cutoff energy of 550 eV throughout the computations. These settings ensure convergence of the total energies to within 1 meV per atom. Structure relaxation proceeded until all forces on atoms were less than 1 meV $Å^{-1}$ and the total stress tensor was within 0.01 GPa of the target value.

3. Results and discussion

3.1. Synthesis and structural characterization

In principle, TA can be incorporated into the carbon nitride framework by copolymerization. A plausible reaction mechanism is illustrated in Fig. S1. The chemical structure of U-CN and modified TCN-x samples were firstly characterized by XRD patterns and FT-IR spectroscopy. As shown in Fig. 1a, the chemical structures of prepared samples are very similar. Two distinct peaks located at 13.0° and 27.4° corresponding to the (1 0 0) and (0 0 2) phase, respectively. The (1 0 0) phase corresponds to the in-plane periodic repeat units of heptazine, while the (0 0 2) phase is attributed to the interlayer aromatic stacking of the CN layers. The peaks gradually weakened with TA modified and the peak of (0 0 2) shifts to smaller angles on going from TCN-0.01 to TCN-0.1, which indicated that TA can be copolymerization with urea, causing the loss of crystallinity and well-ordered CN network structure.[47] The FT-IR spectra (Fig. 1b) for all samples exhibit the distinctive stretch modes of CN heterocycles at 1200–1600 cm^{-1} and the breathing mode of triazine units at 802 cm^{-1}, indicating that the structure of g-C_3N_4 was kept. The wide bands at 3000–3300 cm^{-1} are the typical stretching modes of N–H or O–H stretching, which are attributed to the surface NH_2 group and H_2O molecules, respectively. Solid-state ^{13}C NMR measurements were utilized to further study the structure of U-CN and TCN-x samples (Fig. 1c and d). The samples showed two strong peaks at 164.5 and 156.6 ppm, which can be attributed to the carbon atoms in terminal N_2–C–NH_2 groups and the internal C–N_3 groups, respectively [46]. The ^{13}C NMR peaks of TCN-0.03 is similar to the U-CN due to the TA content is smaller than urea. However, the distinct peaks intensity of TCN-0.03 was weaker with respect to the U-CN. As shown in Fig. 1d, an apparent shift of the N_2–C–NH_2 groups from δ = 164.5 for U-CN to δ = 164.0 ppm for TCN-0.1 was observed, which can be ascribed to S doped onto the framework of the U-CN and the interaction between C and S atoms (the Pauling electronegativity of the doped S atom (2.58) was lower than that of the replaced N atom (3.04)) [57].

XPS measurements were further conducted to study the chemical composition and chemical environments of U-CN and TCN samples. As can be seen form Fig. 2a, the XPS survey of U-CN and TCN-0.03 shows the presence of C, N, O and small amount of S for the TCN-0.03. In Fig. 2b, the C 1s of U-CN and TCN samples can be fitted with two peaks at 288.2 and 284.8 eV, which were corresponded to the N–C=N bonds and the sp^2 C–C bonds in carbon-containing aromatic rings, respectively. The area ratios of the two peaks at 284.8 and 288.2 eV were measured to be 0.037 and 0.080 for U-CN and TCN-0.03, respectively. The result indicates that the TA molecular was doped in CN framework successfully. The N 1s peak can be divided into three distinct peaks at 398.4, 399.2, 400.5 and 404.5 eV in Fig. 2c. The main peak at 398.5 eV is assigned to the sp^2 hybridized nitrogen peak of triazine rings (C–N=C), whereas the peak at 399.2 eV is related to the tertiary N bonded to carbon atoms [41]. The peak at 400.5 eV is assigned to the residual amino functional groups, while the small peak at 404.5 eV is ascribed to charge localization in the heterocycles. Fig. 2d shows the S 2p peak of TCN-0.03, which can be split into four peaks at 161.6 eV, 163.4 eV, 164.5 eV and 167.1 eV. The strong peak at 163.4 eV is from the sulfur-doping by replacing nitrogen atoms to form C-S bonds and the peak at 164.5 eV is attributed to the C–S–C bonds [58]. The weak peak at 167.1 eV is ascribed to sulfur oxide in calcination. In addition, the formation of U-CN and TCN-x were also confirmed by organic elemental analysis (OEA) (Table S1). U-CN has the carbon to nitrogen (C/N) mass ratio of 0.571. While the C/N mass ratio of TCN-0.03 and TCN-0.05 is 0.582 and 0.590, respectively. The results of XPS and OEA analyses are similar to the previous literature [59]. The results of above characterizations demonstrated the well preserve of the chemical structure and skeleton of U-CN in the TCN samples.

The effect of TA on morphology can be observed in the SEM and TEM images of U-CN and TCN samples. In Fig. 3a, the U-CN shows the classical nanosheet-like structure with the smooth surface. When the amount of TA increased from 0.03 to 0.05 g, the structure of TCN changed to partially curled with some irregular pores (Fig. 3b and c). The partially curled morphology may suitable for charges transfer and catalytic reactions [60]. The element mapping results also demonstrate that the TCN sample is formed by C, N, and small amounts of O and S (Fig. S2). From the EDS analysis, the surface mole ratio of C/N is 0.71 and 0.78 for TCN-0.03 and TCN-0.05, respectively, which is good accordance with the elemental and XPS surface analysis. The change of morphology influenced BET surface area. The adsorption isotherms indicated that U-CN and TCN-0.03 contained mesopores (a type IV behavior with an H1 type hysteresis loop was observed) (Fig. S3). The surface area of U-CN was 58 $m^2 g^{-1}$. While the surface area of TCN-0.03 decreased to 40 $m^2 g^{-1}$ due to the curled structure [61]. The TEM image further demonstrated the nanotube-like and pores structure of TCN samples. Fig. 3d shows that the U-CN sample is composed of thin layers. Fig. 4e and f illustrates that the TCN sample is also composed of thin layers but with some irregular pores (the average diameter was 40–80 nm). The curl and pore structure of TCN samples may benefit the light absorption and provide more reactive reaction sites for the reactive species, which may contribute to enhanced photocatalytic activity [47].

3.2. DFT calculations and band structures

To evaluate the effect of TA on the optimization of the optical properties, the light absorption behavior of U-CN and TCN-x samples was then examined by UV–Vis diffusive reflection spectra (DRS) test. In Fig. 4a, U-CN shows light absorption below 470 nm. Whereas, the absorption edge of TCN-x samples shows a remarkable redshift of optical absorption in visible light region from 450 to 700 nm with the insertion of TA. The sufficient light absorption was critical to the activity of photocatalyst since an increased number of incident photons can be used in the photocatalytic process [62]. The band gap of TCN-x samples can be measured from the following formula $\alpha h\nu = A\ (h\nu - E_g)^{n/2}$, where α, h, ν, A, and E_g are the absorption coefficient, Planck's constant, light frequency, a constant, and band gap energy, respectively. It is observed that the band gap of U-CN is 2.66 eV, which in agreement with previous results in Fig. 4b. For the TCN-x samples, the band gap was decreased as the TA contents increased and the band gap of TCN-0.03 is 2.22 eV. The result indicates that the band gap of TCN samples can be easily tuned by TA modification. The positive slope of Mott–Schottky demonstrated the U-CN and TCN-0.03 are n-type semiconductors in Fig. 5c. The flat band potential of samples was calculated by Mott–Schottky analysis at frequency of 1000 Hz, which is -1.13 and −1.03 V versus Ag/AgCl for U-CN and TCN-0.03, respectively. From valence band-XPS, the positions of the VB edge maxima of U-CN and TCN-0.03 are located at 2.17 and 1.95 V in Fig. S4. From the band positions in Fig. 5d, we can find that the light absorption of TCN-0.03 was modified and the negative band was still negative enough for water reduction (the potential of H^+/H_2 was about −0.59 V vs. Ag/AgCl) [63,64].

In order to understand the relationship between the modification of TA and the band gap of U-CN, densities of state (DOS) for U-CN and TCN structure were showed in Fig. 5a and c. For U-CN, the conduction band minimum (CBM) and the valence band minimum (VBM) are all composed of C 2p, N 2s and N 2p. And the total DOS indicates that the E_g is about 2.71 eV (Fig. 5b), which is similar to the previous experiment results [23]. For TCN, the molecular of TA would participate in the framework structure of carbon nitride. And the CBM and VBM of TCN are composed of C 2p, N 2s, N 2p, S 3s, and S 3p. The band gap of TCN was narrower than U-CN, and the value is 1.82 eV (Fig. 5d). The results indicate that DFT calculations can provide fundamental insights into the mechanism by which doping can improve the band structure of g-C_3N_4.

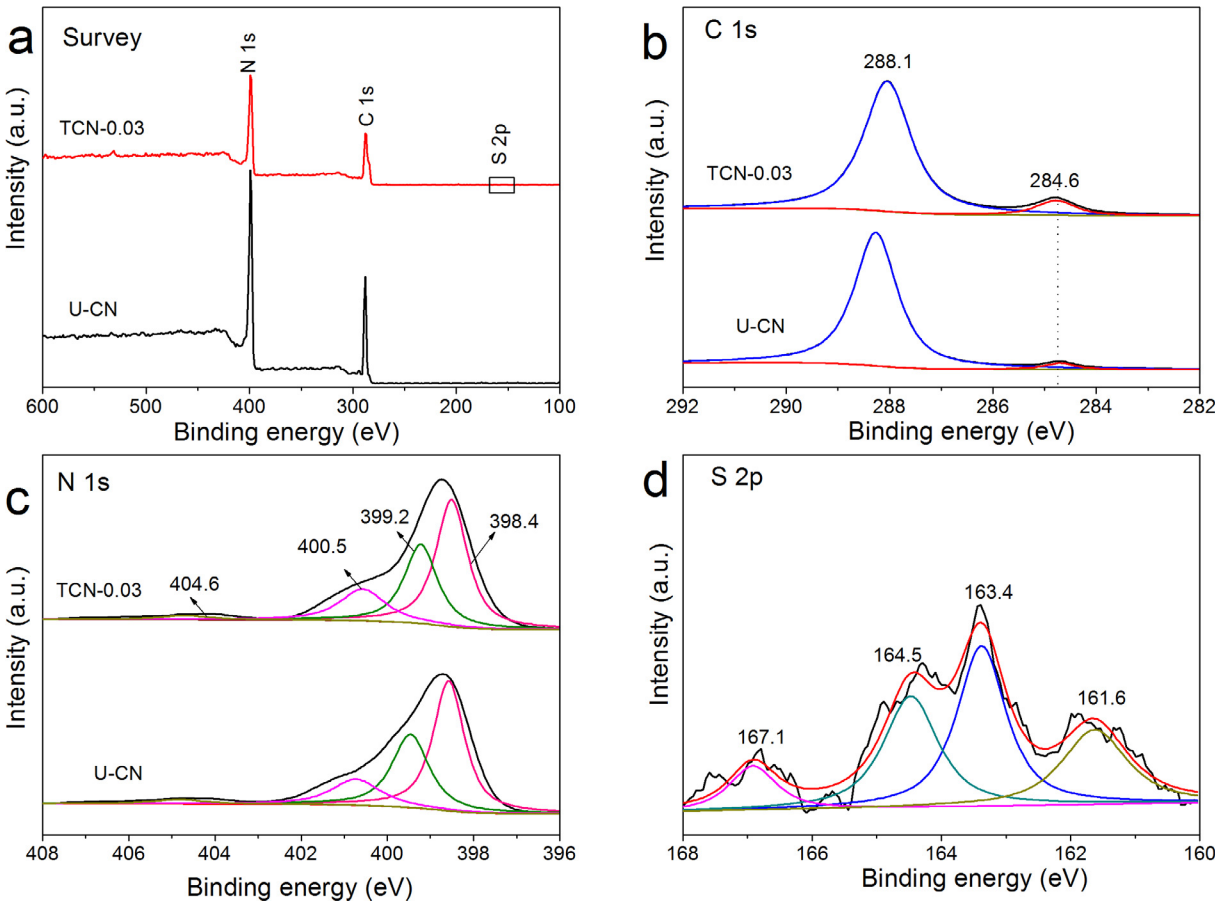

Fig. 2. High-resolution XPS spectra of (a) survey, (b) C 1s, (c) N 1s of the U-CN and TCN-0.03 and (d) S 2p of TCN-0.03.

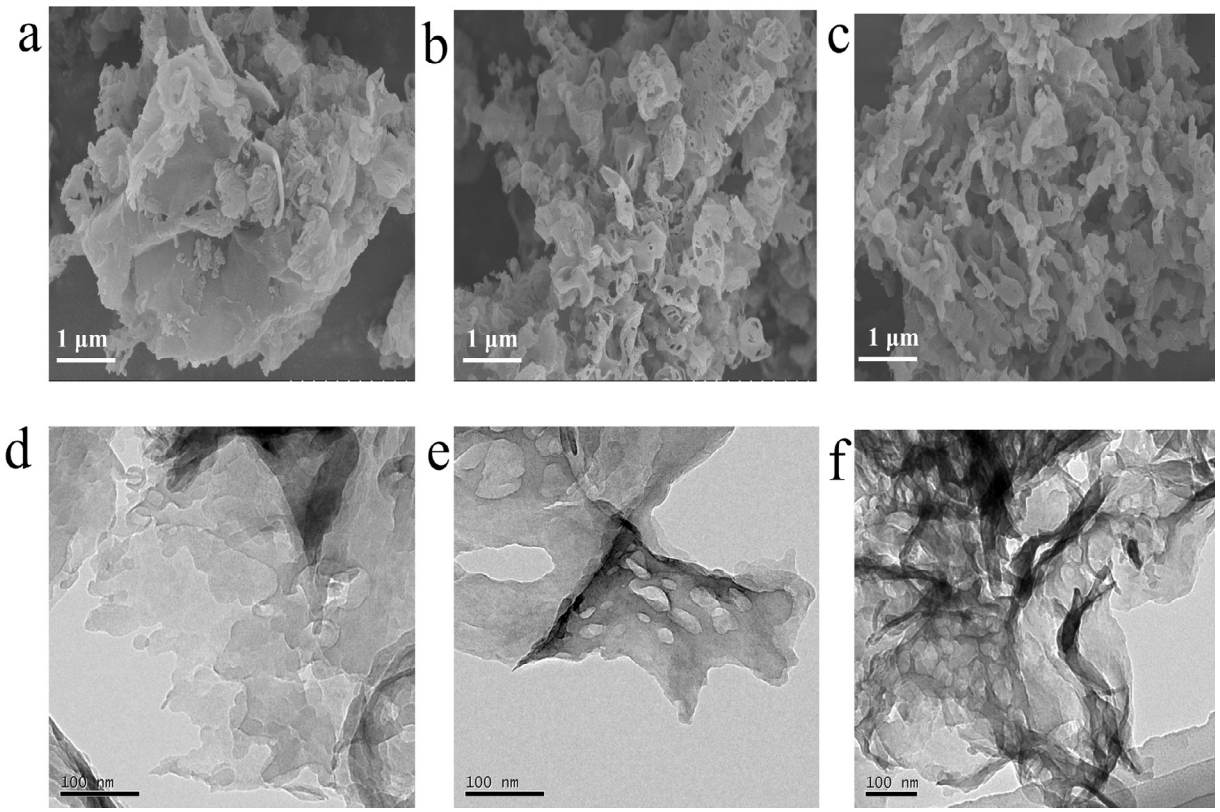

Fig. 3. SEM images of (a) U-CN, (b) TCN-0.03 and (c) TCN-0.05 samples. TEM images of (d) U-CN, (e) TCN-0.03 and (f) TCN-0.05 samples.

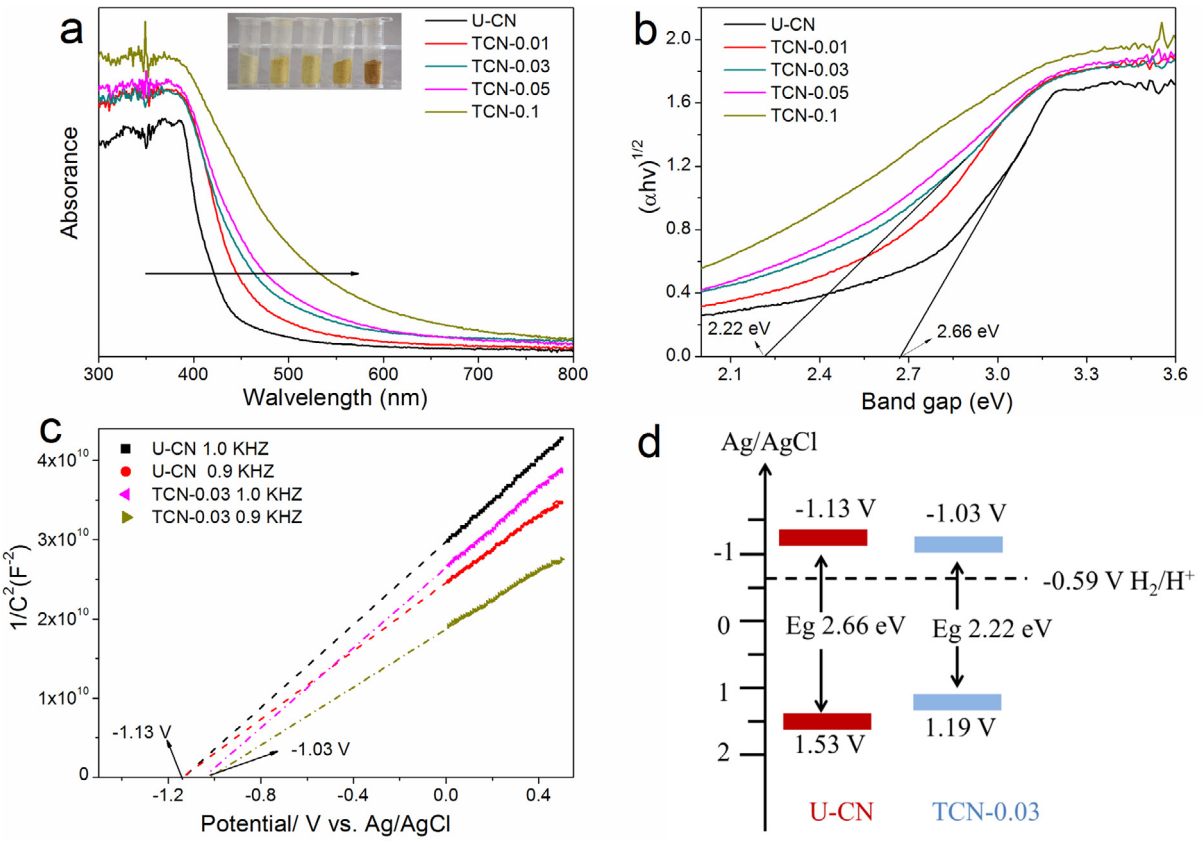

Fig. 4. (a) UV–vis diffraction reflectance spectra (DRS) of the samples, (b) Band gap of the samples, (c) Mott–Schottky plots of U-CN and TCN-0.03 in 0.2 M Na_2SO_4, and (d) Conduction and valence band positions of U-CN and TCN-0.03.

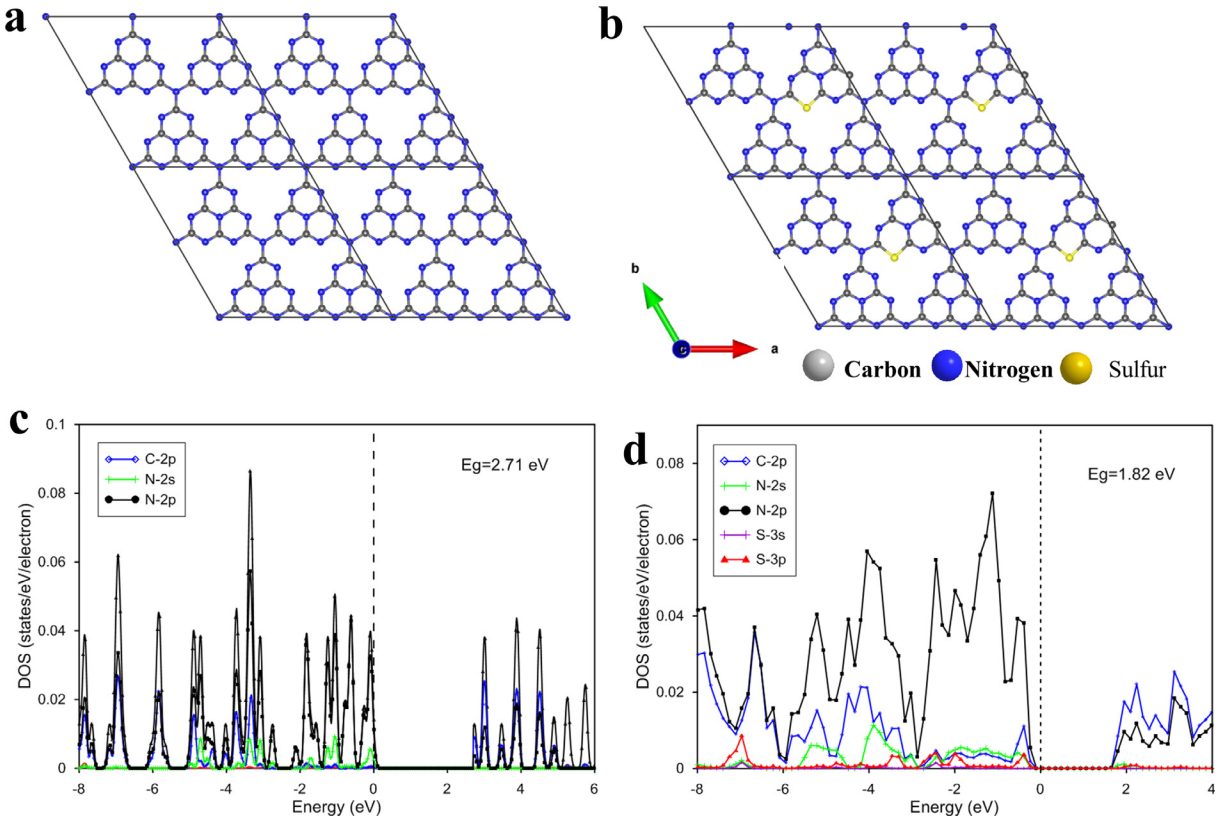

Fig. 5. Structure models of (a) U-CN and (b) TCN, Corresponding DOS of (c) U-CN and (d) TCN.

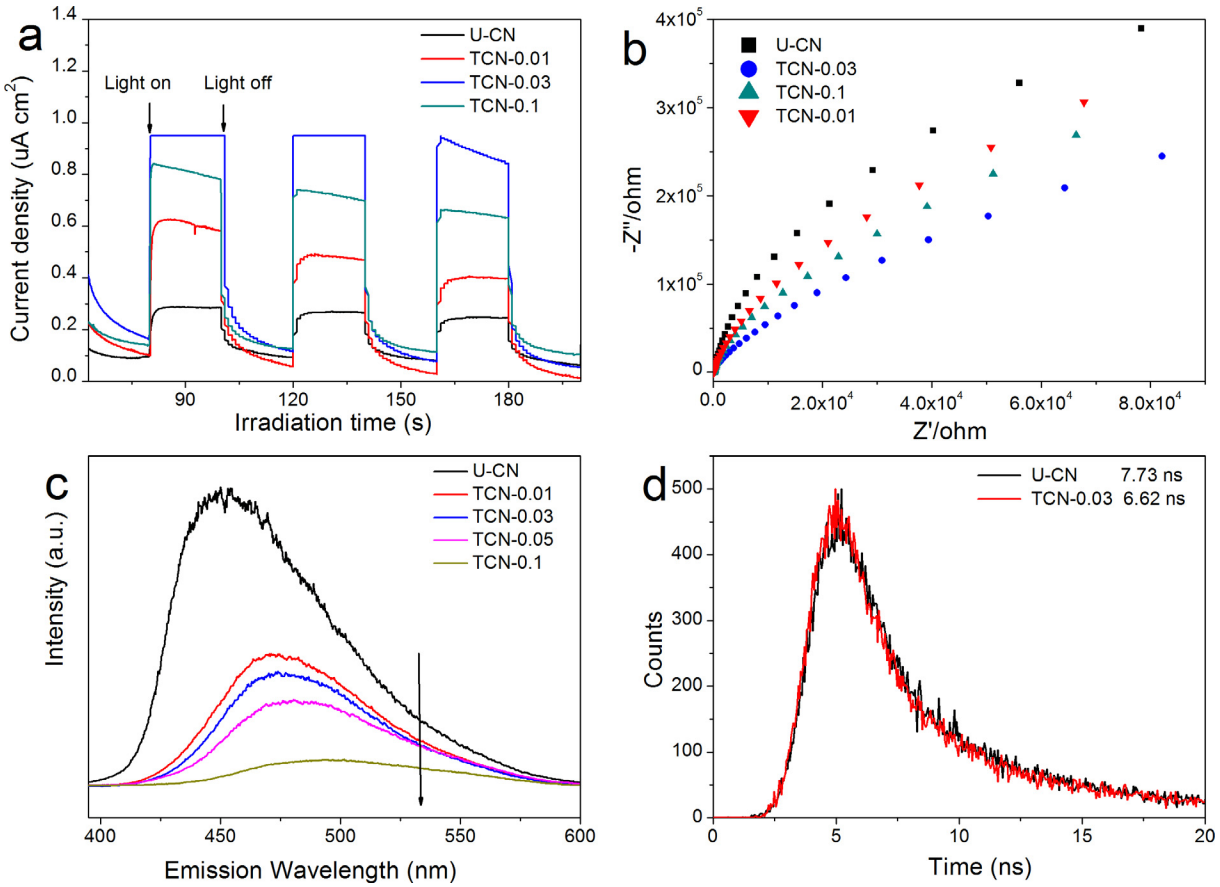

Fig. 6. (a) Transient photocurrent, (b) electrochemical impedance spectroscopy (EIS) Nyquist plots, and (c) photoluminescence (PL) emission spectra of U-CN and TCN samples; (d) time-resolved transient PL decay of U-CN and TCN-0.03 samples.

3.3. Photoelectrochemical measurements and time resolved fluorescence spectra

The separation of holes and electrons are very important in photocatalytic process, which can be evaluated by photocurrent density and EIS. As can be seen in Fig. 6a, all samples are stable in the cycle of light on and light off. Among the tested samples, the TCN-0.03 shows the largest photocurrent. The photocurrent density of TCN-0.03 (0.85 μA cm^{-2}) shows a 4-fold enhancement of photocurrent with respect to the U-CN (0.21 μA cm^{-2}), indicating an improved charge separation. The EIS analysis was conducted in Fig. 6b. The arc radius of EIS spectrum indicates the internal and the surface of photocatalyst. Under dark condition, the optimized TCN-0.03 sample present smaller resistances than the U-CN. The above electronic properties indicate that TA modification could enhance efficiency of the charge transfer process, leading to the enhancement of photocatalytic activity.

PL is a useful technique in studying the generation, transfer, and recombination of carriers. Fig. 6c shows the room temperature PL spectra of the sample. Interestingly, the narrowed band gap doesn't bring higher recombination efficiency of photogenerated carriers. The strong emission peak center of U-CN located at 451 nm may attribute to the $\pi \rightarrow \pi^*$ electronic transitions in the conjugated heptazine system units [36]. The wavelength of TCN samples was longer with respect to U-CN (from 450 nm to 482 nm). Compared to U-CN, the TCN samples exhibits decreased emission intensity obviously. Thus the rate of charge recombination can be suppressed by copolymerization. Time resolved fluorescence spectra were further employed to investigate the charge separation of the samples in Fig. 6d. The fitting results are given in Table 1. The lifetime of TCN-0.03 is shorten than that of U-CN, with the average lifetimes of about 7.73 and 6.62 ns for U-CN and TCN-0.03, respectively. The decreased singlet exciton lifetime of the optimized samples obviously implies enhanced exciton dissociation [65]. The well electronic and optical properties of TCN samples from TA modification would promote the photocatalytic activities.

Table 1
The fitted fluorescence decay components of U-CN and TCN-0.03, respectively.

Samples	Decay time/ns		Relative amplitude/%		Average lifetime/ns
	t1	t2	B1	B2	
U-CN	2.4057	8.9107	45.18	54.82	7.73
TCN-0.03	2.0795	7.4675	40.26	59.74	6.62

3.4. Photocatalytic performance

3.4.1. Photocatalytic degradation of SMZ

The photocatalytic degradation activities of the obtained samples were further evaluated in terms of SMZ antibiotics removal in aqueous solution. Previous studies have shown that SMZ is very stable and could not be photolyzed under light irradiation in the absence of photocatalysts [66]. With the photocatalyst, SMZ can react with the radical species and be degraded to small molecular organics or other inorganic compounds. Before irradiation, adsorption/desorption equilibrium between the photocatalyst and pollutants in aqueous solution was reached in 60 min (Table S2). The concentration of SMZ decreased faster for the TCN samples followed by U-CN in Fig. 7a. U-CN showed limited photocatalytic activity, and the degradation efficiency was 58% after illumination for 1 h. For the TCN samples, the degradation efficiency increased from 58% to 97% as the amount of TA increased from 0 to

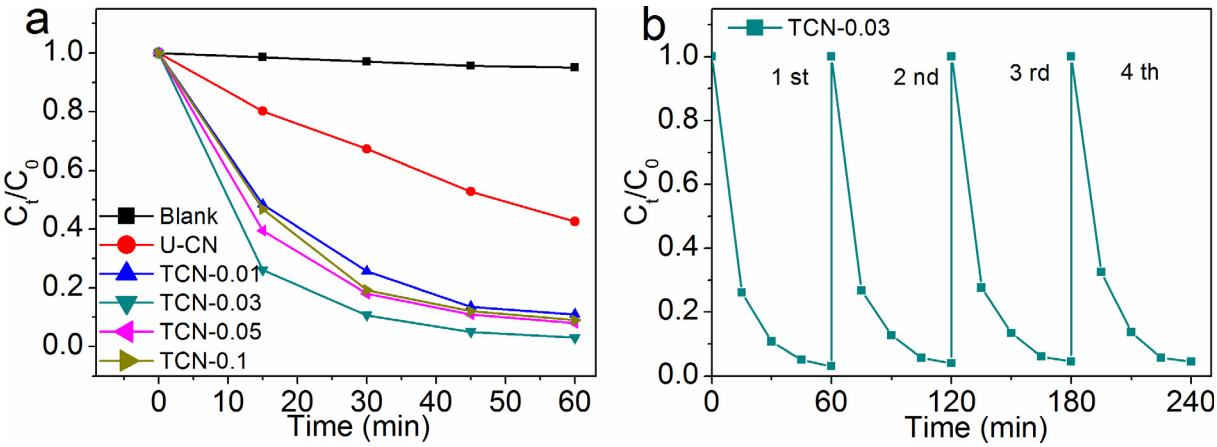

Fig. 7. (a) Photocatalytic degradation of SMZ (C_0 = 10 mg L^{-1}) over U-CN and TCN samples under visible light irradiation and (b) Cycle runs of TCN-0.03 photocatalyst for degradation of SMZ.

30 mg. However, When the content of TA increased to 100 mg, the degradation efficiency decreased. This finding indicates that excessive dopant destructs the conjugated structures of carbon nitride. The results were also indicated that the degree of polymerization must be appropriately controlled for promoting the photocatalytic activity of carbon nitride [67,68]. As shown in Fig. S5, the rate constant (k) value of TCN-0.03 is 0.058 min^{-1}, which is 4.2 times higher than that of U-CN. The stability of photocatalyst was showed in Fig. 7b. Furthermore, after photocatalytic degradation reactions, the used TCN-0.03 sample was further subjected to structural characterizations by XRD, FTIR and SEM. As displayed in Fig. S6, no obvious change in the structure is observed when the polymers are collected and characterized by XRD and FTIR, which confirms the high stability of TA modified CN photocatalyst. In addition, the structure remains well constructed even after several cycle reactions in Fig. S7. To fully understand the degradation products of SMZ by the TCN photocatalytic reaction, high performance liquid–mass spectrometer (HPLC–MS) were further performed to identify the oxidation products of SMZ. The *m/z* of SMZ was 279 in Fig. S8a. With the prolongation of irradiation time, SMZ was degraded gradually. As shown in Fig. S8b, four main products were detected by HPLC–MS. The products for the photodegradation of SMZ have been listed in Table S3.

3.4.2. Photocatalytic hydrogen (H_2) evolution experiments

To evaluate the photocatalytic activity of the as-prepared photocatalysts, hydrogen evolution experiments from water splitting were carried out under visible light irradiation with triethanolamine (TEOA) as sacrificial agent and 3 wt% Pt as cocatalyst, respectively. As shown in Fig. 8a, all the TCN samples show largely enhanced H_2 generation activity. The photocatalytic activities depend on the amounts of TA added. Small amounts of TA added in urea can largely enhance the photocatalytic activities, such as 0.01–0.05 g TA in 10 g urea. Among the test samples, TCN-0.03 presents the highest evolution rate reaching 55 μmol h^{-1}, which is nearly 11 times higher than the U-CN (5 μmol h^{-1}). Further increasing the addition amount of TA will cause the H_2 evolution rate decrease. But the H_2 evolution rate of TCN-0.1 was still higher than that of the U-CN, which indicated that TA modification was beneficial to improving the photocatalytic activity. After the normalization of hydrogen generation rate by surface area, the TCN-0.03 still showed higher activity than other samples indicating that the modified of TA improved the catalytic activity of each active site.

To confirm the stability of H_2 generation by TCN-0.03, the photocatalytic reaction was tested for 12 h in Fig. 8b. The result exhibits that the high photocatalytic H_2 production activity of TCN-0.03 is well kept at every cycle, indicating the high stability of the catalyst. The apparent quantum yield (AQY) for H_2 evolution of TCN-0.03 was investigated under various monochromatic light irradiation conditions in Fig. S9. The AQY results of TCN-0.03 revealed that the trend of the yield of H_2 corresponds well with DRS spectrum. The production of H_2 decrease with the increase in incident wavelength, and the AQY reached 4.8% under light of 420 nm irradiation. The photocatalytic activity can be observed even at 500 nm, suggesting that the harvested visible photons

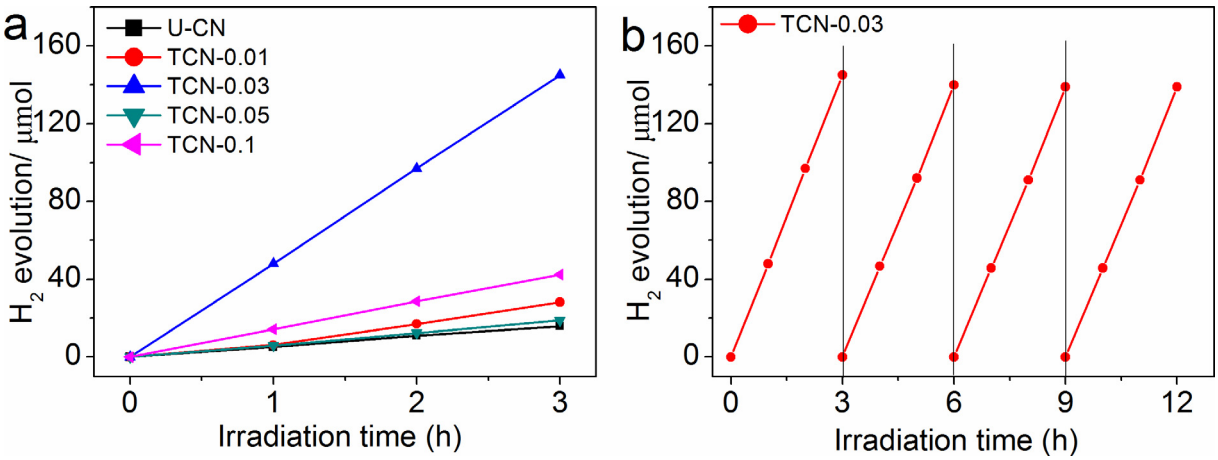

Fig. 8. (a) Photocatalytic H_2 evolution activities of U-CN and TCN samples under visible light irradiation and (b) Cycle test H_2 evolution of TCN-0.03 sample under visible light irradiation.

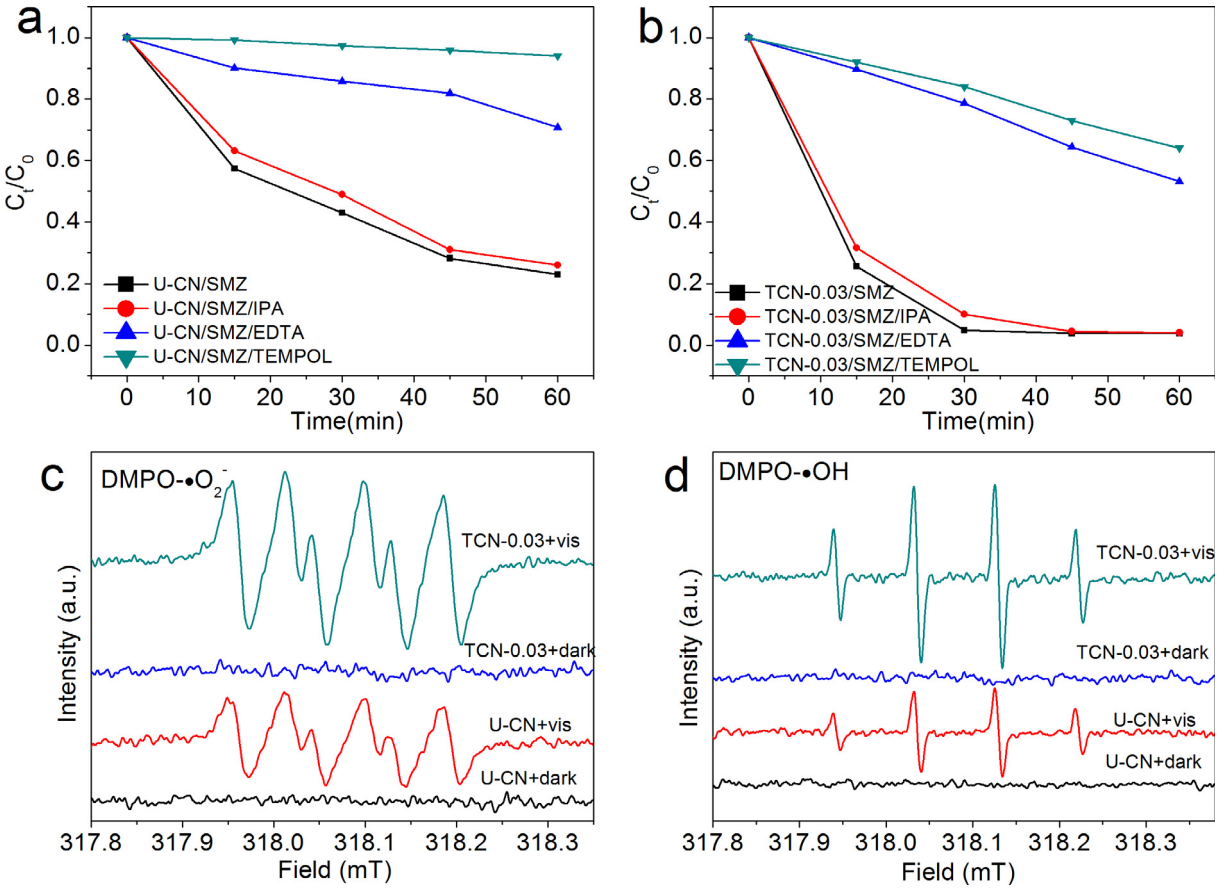

Fig. 9. (a) The photocatalytic degradation plots of SMZ over U-CN and (b) TCN-0.03 with the addition of hole, $\cdot O_2^-$ and ·OH radical scavenger under visible light irradiation; (c) DMPO ESR spectra in dark and under visible-light ($\lambda \geq 420$ nm) for 8 min in methanol dispersion, respectively for $\cdot O_2^-$ and (d) aqueous dispersion for ·OH.

were obtained of TCN-0.03. Moreover, the result of AQY was higher than that of other carbon nitride samples (Table S4).

3.5. Photocatalytic mechanism

The reactive radicals were important for photocatalytic oxidation reaction. In order to investigate the role of reactive species in the degradation process, radical trapping experiments have been carried out. The scavenger used are ethylenediaminetetraacetic acid disodium salt (EDTA-2Na) for hole, TEMPOL for $\cdot O_2^-$ scavenger, and isopropanol (IPA) for hydroxyl radical (·OH). In Fig. 9a and b, the removal rate of SMZ show a significant decrease in the presence of TEMPOL and EDTA-2Na, while only weak in IPA, suggesting that the $\cdot O_2^-$ and hole are the main radical species in the degradation process. ESR spin-trapping method was carried out to further confirm the reactive species over samples in photocatalytic process. The signals of DMPO-$\cdot O_2^-$ for TCN-0.03 and U-CN were shown in Fig. 9c. For TCN-0.03 composite, it exhibited much higher signal intensity than U-CN under visible light, which indicates that O_2 obtaining more electrons to produce more $\cdot O_2^-$. In Fig. 9d, no signals of ·OH could be observed over samples in dark environment. Weak signals of U-CN can be found while light irradiation. The increased intensities of ·OH was also observed in TCN-0.03, which can be resulted from the reduction of $\cdot O_2^-$. The results suggest that more $\cdot O_2^-$ and ·OH generated in the TCN-0.03 accounted for the photocatalytic activity enhancement.

On the basis of the above results, a possible mechanism for the degradation of SMZ was proposed in Fig. 10. For U-CN, it is suggested that electrons are excited from the VB to CB and left holes in the VB. After TA copolymerizing with urea, TA molecular was doping in the U-CN framework, which shows the enhanced optical absorption. Therefore, more visible light can be utilized for the TCN. In addition, the wrinkle and porous structure of TCN was also beneficial to the efficiency of photogenerated electron-hole pairs [69]. The electrons on the TCN could transfer from the interior to the surface of the TCN along the porous structure [70,71]. For H_2 evolution, when the holes were trapped by TEOA, the electrons on TCN can be coupled with the Pt, and further react with water. In this process, the photocatalytic activity enhancement of TCN samples for SMZ degradation and H_2 evolution could be attributed to synergetic effects of sufficient optical absorption, well photoelectronic properties and distinct wrinkle and porous structure.

4. Conclusions

In summary, we have demonstrated a facile and economical method to enhance carbon nitride activity via copolymerization of urea and TA for photocatalytic degradation and water splitting. After TA modification, the chemical composition was minor change, while the optical absorption, electronic properties and nanostructure were optimized. The rational design of TCN samples improve the charge migration and separation and enhanced visible light absorption (above 520 nm), which was beneficial to enhance the photocatalytic activity. In addition, the charge carrier transfer and separation of TCN was improved due to the wrinkle porous structure and the disorder-order junction. As a result, the optimized TCN-0.03 sample exhibited high efficiency in hydrogen evolution with sacrificial agent, which was about 11 times than that of U-CN. Also, the TCN-0.03 could decompose SMZ in 60 min with a high reaction rate of 0.058 min^{-1}, which was highly efficient

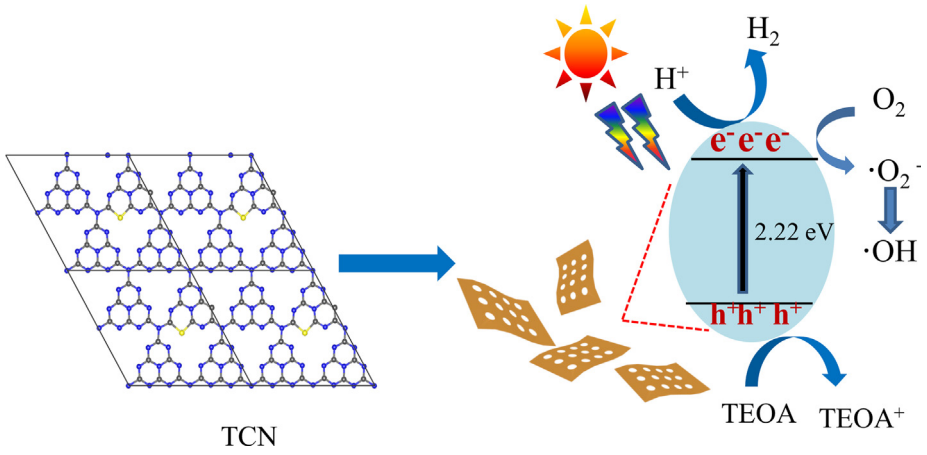

Fig. 10. Possible mechanism for pollutant degradation, electron flow and water splitting by TCN sample.

than U-CN. Moreover, the $\cdot O_2^-$ and holes are the main radical species in the degradation process of SMZ for TCN-0.03 sample. This work suggests a facile self-assembly method to design the different band structure photocatalytic material by copolymerization for water splitting and pollutants degradation.

Acknowledgements

The authors would like to thank Ning Yan for his assistance with the TEM measurements, and Shuqu Zhang for his assistance with the DRS measurements. This study was financially supported by the Program for the National Natural Science Foundation of China (51579098, 51779090, 51709101, 51278176, 51521006, 51378190, 51408206), the National Program for Support of Top-Notch Young Professionals of China (2014), the Fundamental Research Funds for the Central Universities, Hunan Provincial Science and Technology Plan Project (No. 2017SK2243), Shanghai Tongji Gao Tingyao Environmental Science and Technology Development Foundation, Hunan Provincial Innovation Foundation For Postgraduate, the Program for New Century Excellent Talents in University (NCET-13-0186), the Fundamental Research Funds for the Central Universities (531107051080), and the Program for Changjiang Scholars and Innovative Research Team in University (IRT-13R17).

Appendix A. Supplementary data

Supplementary data to this article can be found online at https://doi.org/10.1016/j.cej.2018.11.140.

References

[1] J.-L. Gong, B. Wang, G.-M. Zeng, C.-P. Yang, C.-G. Niu, Q.-Y. Niu, W.-J. Zhou, Y. Liang, Removal of cationic dyes from aqueous solution using magnetic multi-wall carbon nanotube nanocomposite as adsorbent, J. Hazard. Mater. 164 (2009) 1517–1522.
[2] M. Chen, P. Xu, G. Zeng, C. Yang, D. Huang, J. Zhang, Bioremediation of soils contaminated with polycyclic aromatic hydrocarbons, petroleum, pesticides, chlorophenols and heavy metals by composting: applications, microbes and future research needs, Biotechnol. Adv. 33 (2015) 745–755.
[3] M. Cheng, G. Zeng, D. Huang, C. Lai, P. Xu, C. Zhang, Y. Liu, Hydroxyl radicals based advanced oxidation processes (AOPs) for remediation of soils contaminated with organic compounds: a review, Chem. Eng. J. 284 (2016) 582–598.
[4] J. Liang, Z. Yang, L. Tang, G. Zeng, M. Yu, X. Li, H. Wu, Y. Qian, X. Li, Y. Luo, Changes in heavy metal mobility and availability from contaminated wetland soil remediated with combined biochar-compost, Chemosphere 181 (2017) 281–288.
[5] J. Wan, G. Zeng, D. Huang, L. Hu, P. Xu, C. Huang, R. Deng, W. Xue, C. Lai, C. Zhou, K. Zheng, X. Ren, X. Gong, Rhamnolipid stabilized nano-chlorapatite: synthesis and enhancement effect on Pb-and Cd-immobilization in polluted sediment, J. Hazard. Mater. 343 (2018) 332–339.
[6] X. Gong, D. Huang, Y. Liu, G. Zeng, R. Wang, J. Wan, C. Zhang, M. Cheng, X. Qin, W. Xue, Stabilized nanoscale zerovalent iron mediated cadmium accumulation and oxidative damage of Boehmeria nivea (L.) Gaudich cultivated in cadmium contaminated sediments, Environ. Sci. Technol. 51 (2017) 11308–11316.
[7] P. Xu, G.M. Zeng, D.L. Huang, C.L. Feng, S. Hu, M.H. Zhao, C. Lai, Z. Wei, C. Huang, G.X. Xie, Z.F. Liu, Use of iron oxide nanomaterials in wastewater treatment: a review, Sci. Total Environ. 424 (2012) 1–10.
[8] W.-W. Tang, G.-M. Zeng, J.-L. Gong, J. Liang, P. Xu, C. Zhang, B.-B. Huang, Impact of humic/fulvic acid on the removal of heavy metals from aqueous solutions using nanomaterials: a review, Sci. Total Environ. 468 (2014) 1014–1027.
[9] P. Xu, G.M. Zeng, D.L. Huang, C. Lai, M.H. Zhao, Z. Wei, N.J. Li, C. Huang, G.X. Xie, Adsorption of Pb II) by iron oxide nanoparticles immobilized Phanerochaete chrysosporium: equilibrium, kinetic, thermodynamic and mechanisms analysis, Chem. Eng. J. 203 (2012) 423–431.
[10] Y. Zhang, G.-M. Zeng, L. Tang, D.-L. Huang, X.-Y. Jiang, Y.-N. Chen, A hydroquinone biosensor using modified core–shell magnetic nanoparticles supported on carbon paste electrode, Biosens. Bioelectron. 22 (2007) 2121–2126.
[11] P. Hu, H. Su, Z. Chen, C. Yu, Q. Li, B. Zhou, P.J.J. Alvarez, M. Long, Selective degradation of organic pollutants using an efficient metal-free catalyst derived from carbonized polypyrrole via peroxymonosulfate activation, Environ. Sci. Technol. 51 (2017) 11288–11296.
[12] X. Tan, Y. Liu, G. Zeng, X. Wang, X. Hu, Y. Gu, Z. Yang, Application of biochar for the removal of pollutants from aqueous solutions, Chemosphere 125 (2015) 70–85.
[13] J.-H. Deng, X.-R. Zhang, G.-M. Zeng, J.-L. Gong, Q.-Y. Niu, J. Liang, Simultaneous removal of Cd(II) and ionic dyes from aqueous solution using magnetic graphene oxide nanocomposite as an adsorbent, Chem. Eng. J. 226 (2013) 189–200.
[14] F. Long, J.-L. Gong, G.-M. Zeng, L. Chen, X.-Y. Wang, J.-H. Deng, Q.-Y. Niu, H.-Y. Zhang, X.-R. Zhang, Removal of phosphate from aqueous solution by magnetic Fe–Zr binary oxide, Chem. Eng. J. 171 (2011) 448–455.
[15] C. Zhang, C. Lai, G. Zeng, D. Huang, L. Tang, C. Yang, Y. Zhou, L. Qin, M. Cheng, Nanoporous Au-based chronocoulometric aptasensor for amplified detection of Pb2+ using DNAzyme modified with Au nanoparticles, Biosens. Bioelectron. 81 (2016) 61–67.
[16] L. Hu, J. Wan, G. Zeng, A. Chen, G. Chen, Z. Huang, K. He, M. Cheng, C. Zhou, W. Xiong, C. Lai, P. Xu, Comprehensive evaluation of the cytotoxicity of CdSe/ZnS quantum dots in Phanerochaete chrysosporium by cellular uptake and oxidative stress, Environ. Sci. Nano (2017).
[17] J. Li, X. Wu, W. Pan, G. Zhang, H. Chen, Vacancy-rich monolayer BiO2−x as a highly efficient UV, visible, and near-infrared responsive photocatalyst, Angew. Chem. 130 (2018) 500–504.
[18] J. Zhang, T. Wang, X. Chang, A. Li, J. Gong, Fabrication of porous nanoflake BiMOx (M = W, V, and Mo) photoanodes via hydrothermal anion exchange, Chem. Sci. 7 (2016) 6381–6386.
[19] J. Qin, L. Lin, X. Wang, A perovskite oxide $LaCoO_3$ cocatalyst for efficient photocatalytic reduction of CO_2 with visible light, Chem. Commun. (Cambridge) 54 (2018) 2272–2275.
[20] X. Zhou, C. Lai, D. Huang, G. Zeng, L. Chen, L. Qin, P. Xu, M. Cheng, C. Huang, C. Zhang, C. Zhou, Preparation of water-compatible molecularly imprinted thiol-functionalized activated titanium dioxide: selective adsorption and efficient photodegradation of 2, 4-dinitrophenol in aqueous solution, J. Hazard. Mater. 346 (2018) 113–123.
[21] D. Huang, R. Deng, J. Wan, G. Zeng, W. Xue, X. Wen, C. Zhou, L. Hu, X. Liu, P. Xu, X. Guo, X. Ren, Remediation of lead-contaminated sediment by biochar-supported nano-chlorapatite: accompanied with the change of available phosphorus and organic matters, J. Hazard. Mater. 348 (2018) 109–116.
[22] H. Wang, Y. Wu, X. Yuan, G. Zeng, J. Zhou, X. Wang, J.W. Chew, Clay-inspired MXene-based electrochemical devices and photo-electrocatalyst: state-of-the-art progresses and challenges, Adv. Mater. 30 (2018) 1704561.
[23] Q. Zheng, D.P. Durkin, J.E. Elenewski, Y. Sun, N.A. Banek, L. Hua, H. Chen, M.J. Wagner, W. Zhang, D. Shuai, Visible-light-responsive graphitic carbon nitride: rational design and photocatalytic applications for water treatment, Environ. Sci. Technol. 50 (2016) 12938–12948.
[24] C. Zhou, C. Lai, P. Xu, G. Zeng, D. Huang, C. Zhang, M. Cheng, L. Hu, J. Wan, Y. Liu, W. Xiong, Y. Deng, M. Wen, In situ grown AgI/$Bi_{12}O_{17}Cl_2$ heterojunction

photocatalysts for visible light degradation of sulfamethazine: efficiency, pathway, and mechanism, ACS Sustainable Chem. Eng. 6 (2018) 4174–4184.
[25] S. Pasternak, Y. Paz, On the similarity and dissimilarity between photocatalytic water splitting and photocatalytic degradation of pollutants, ChemPhysChem 14 (2013) 2059–2070.
[26] H. Wu, C. Lai, G. Zeng, J. Liang, J. Chen, J. Xu, J. Dai, X. Li, J. Liu, M. Chen, L. Lu, L. Hu, J. Wan, The interactions of composting and biochar and their implications for soil amendment and pollution remediation: a review, Crit. Rev. Biotechnol. 37 (2017) 754–764.
[27] X. Ren, G. Zeng, L. Tang, J. Wang, J. Wan, Y. Liu, J. Yu, H. Yi, S. Ye, R. Deng, Sorption, transport and biodegradation – an insight into bioavailability of persistent organic pollutants in soil, Sci. Total Environ. 610–611 (2017) 1154–1163.
[28] W. Xiong, J. Tong, Z. Yang, G. Zeng, Y. Zhou, D. Wang, P. Song, R. Xu, C. Zhang, M. Cheng, Adsorption of phosphate from aqueous solution using iron-zirconium modified activated carbon nanofiber: performance and mechanism, J. Colloid Interface Sci. 493 (2017) 17–23.
[29] M. Cheng, G. Zeng, D. Huang, C. Lai, Y. Liu, C. Zhang, J. Wan, L. Hu, C. Zhou, W. Xiong, Efficient degradation of sulfamethazine in simulated and real wastewater at slightly basic pH values using Co-SAM-SCS/H_2O_2 Fenton-like system, Water Res. 138 (2018) 7–18.
[30] H. Ou, P. Yang, L. Lin, M. Anpo, X. Wang, Carbon nitride aerogels for the photoredox conversion of water, Angew. Chem. Int. Ed. Engl. 56 (2017) 10905–10910.
[31] Z. He, C. Kim, L. Lin, T.H. Jeon, S. Lin, X. Wang, W. Choi, Formation of heterostructures via direct growth CN on h-BN porous nanosheets for metal-free photocatalysis, Nano Energy 42 (2017) 58–68.
[32] D. Masih, Y. Ma, S. Rohani, Graphitic C_3N_4 based noble-metal-free photocatalyst systems: a review, Appl. Catal. B: Environ. 206 (2017) 556–588.
[33] W.J. Ong, L.L. Tan, Y.H. Ng, S.T. Yong, S.P. Chai, Graphitic carbon nitride (g-C_3N_4)-based photocatalysts for artificial photosynthesis and environmental remediation: are we a step closer to achieving sustainability? Chem. Rev. 116 (2016) 7159–7329.
[34] C. Zhou, C. Lai, C. Zhang, G. Zeng, D. Huang, M. Cheng, L. Hu, W. Xiong, M. Chen, J. Wang, Y. Yang, L. Jiang, Semiconductor/boron nitride composites: synthesis, properties, and photocatalysis applications, Appl. Catal. B: Environ. 238 (2018) 6–18.
[35] W. Che, W. Cheng, T. Yao, F. Tang, W. Liu, H. Su, Y. Huang, Q. Liu, J. Liu, F. Hu, Z. Pan, Z. Sun, S. Wei, Fast Photoelectron transfer in (Cring)–C_3N_4 plane heterostructural nanosheets for overall water splitting, J. Am. Chem. Soc. 139 (2017) 3021–3026.
[36] H. Wang, Y. Wu, M. Feng, W. Tu, T. Xiao, T. Xiong, H. Ang, X. Yuan, J.W. Chew, Visible-light-driven removal of tetracycline antibiotics and reclamation of hydrogen energy from natural water matrices and wastewater by polymeric carbon nitride foam, Water Res. 144 (2018) 215–225.
[37] Y. Wu, H. Wang, W. Tu, Y. Liu, S. Wu, Y.Z. Tan, J.W. Chew, Construction of hierarchical 2D–2D $Zn_3In_2S_6$/fluorinated polymeric carbon nitride nanosheets photocatalyst for boosting photocatalytic degradation and hydrogen production performance, Appl. Catal. B: Environ. 233 (2018) 58–69.
[38] J. Xia, M. Ji, J. Di, B. Wang, S. Yin, Q. Zhang, M. He, H. Li, Construction of ultrathin C_3N_4/$Bi_4O_5I_2$ layered nanojunctions via ionic liquid with enhanced photocatalytic performance and mechanism insight, Appl. Catal. B: Environ. 191 (2016) 235–245.
[39] T. Xiong, W. Cen, Y. Zhang, F. Dong, Bridging the g-C_3N_4 interlayers for enhanced photocatalysis, ACS Catal. 6 (2016) 2462–2472.
[40] G.-H. Moon, M. Fujitsuka, S. Kim, T. Majima, X. Wang, W. Choi, Eco-friendly photochemical production of H_2O_2 through O_2 reduction over carbon nitride frameworks incorporated with multiple heteroelements, ACS Catal. 7 (2017) 2886–2895.
[41] C. Liu, Y. Zhang, F. Dong, A.H. Reshak, L. Ye, N. Pinna, C. Zeng, T. Zhang, H. Huang, Chlorine intercalation in graphitic carbon nitride for efficient photocatalysis, Appl. Catal. B: Environ. 203 (2017) 465–474.
[42] Y. Wu, H. Wang, Y. Sun, T. Xiao, W. Tu, X. Yuan, G. Zeng, S. Li, J.W. Chew, Photogenerated charge transfer via interfacial internal electric field for significantly improved photocatalysis in direct Z-scheme oxygen-doped carbon nitrogen/CoAl-layered double hydroxide heterojunction, Appl. Catal. B: Environ. 227 (2018) 530–540.
[43] Z. Wan, G. Zhang, X. Wu, S. Yin, Novel visible-light-driven Z-scheme Bi_{12} GeO_{20}/g-C_3N_4 photocatalyst: oxygen-induced pathway of organic pollutants degradation and proton assisted electron transfer mechanism of Cr(VI) reduction, Appl. Catal. B: Environ. 207 (2017) 17–26.
[44] M. Zhu, S. Kim, L. Mao, M. Fujitsuka, J. Zhang, X. Wang, T. Majima, Metal-free photocatalyst for H_2 evolution in visible to near-infrared region: black phosphorus/graphitic carbon nitride, J. Am. Chem. Soc. 139 (2017) 13234–13242.
[45] J. Yuan, X. Liu, Y. Tang, Y. Zeng, L. Wang, S. Zhang, T. Cai, Y. Liu, S. Luo, Y. Pei, C. Liu, Positioning cyanamide defects in g-C_3N_4: engineering energy levels and active sites for superior photocatalytic hydrogen evolution, Appl. Catal. B: Environ. 237 (2018) 24–31.
[46] H. Kim, S. Gim, T.H. Jeon, H. Kim, W. Choi, Distorted carbon nitride structure with substituted benzene moieties for enhanced visible light photocatalytic activities, ACS Appl. Mater. Interfaces 9 (2017) 40360–40368.
[47] J. Qin, S. Wang, H. Ren, Y. Hou, X. Wang, Photocatalytic reduction of CO_2 by graphitic carbon nitride polymers derived from urea and barbituric acid, Appl. Catal. B: Environ. 179 (2015) 1–8.
[48] S. Cao, J. Low, J. Yu, M. Jaroniec, Polymeric photocatalysts based on graphitic carbon nitride, Adv. Mater. 27 (2015) 2150–2176.
[49] M. Shalom, S. Inal, C. Fettkenhauer, D. Neher, M. Antonietti, Improving carbon nitride photocatalysis by supramolecular preorganization of monomers, J. Am. Chem. Soc. 135 (2013) 7118–7121.
[50] L. Jiang, X. Yuan, G. Zeng, Z. Wu, J. Liang, X. Chen, L. Leng, H. Wang, H. Wang, Metal-free efficient photocatalyst for stable visible-light photocatalytic degradation of refractory pollutant, Appl. Catal. B: Environ. 221 (2018) 715–725.
[51] C. Zhou, C. Lai, P. Xu, G. Zeng, D. Huang, Z. Li, C. Zhang, M. Cheng, L. Hu, J. Wan, F. Chen, W. Xiong, R. Deng, Rational design of carbon-doped carbon nitride/$Bi_{12}O_{17}Cl_2$ composites: a promising candidate photocatalyst for boosting visible-light-driven photocatalytic degradation of tetracycline, ACS Sustainable Chem. Eng. 6 (2018) 6941–6949.
[52] P. Qiu, C. Xu, H. Chen, F. Jiang, X. Wang, R. Lu, X. Zhang, One step synthesis of oxygen doped porous graphitic carbon nitride with remarkable improvement of photo-oxidation activity: role of oxygen on visible light photocatalytic activity, Appl. Catal. B: Environ. 206 (2017) 319–327.
[53] G. Zhang, A. Savateev, Y. Zhao, L. Li, M. Antonietti, Advancing the n [rightward arrow] [small pi]* electron transition of carbon nitride nanotubes for H_2 photosynthesis, J. Mater. Chem. A 5 (2017) 12723–12728.
[54] Z. Guigang, L. Guosheng, L. Zhi-An, L. Lihua, S. Aleksandr, H. Tobias, Z. Spiros, W. Xinchen, A. Markus, Optimizing optical absorption, exciton dissociation, and charge transfer of a polymeric carbon nitride with ultrahigh solar hydrogen production activity, Angew. Chem. 129 (2017) 13630–13634.
[55] J. Liu, T. Zhang, Z. Wang, G. Dawson, W. Chen, Simple pyrolysis of urea into graphitic carbon nitride with recyclable adsorption and photocatalytic activity, J. Mater. Chem. 21 (2011) 14398–14401.
[56] C.Y. Zhou, C. Lai, D.L. Huang, G.M. Zeng, C. Zhang, M. Cheng, L. Hu, J. Wan, W.P. Xiong, M. Wen, X.F. Wen, L. Qin, Highly porous carbon nitride by supramolecular preassembly of monomers for photocatalytic removal of sulfamethazine under visible light driven, Appl. Catal. B: Environ. 220 (2018) 202–210.
[57] H. Ou, X. Chen, L. Lin, Y. Fang, X. Wang, Biomimetic donor-acceptor motifs in conjugated polymers for promoting exciton splitting and charge separation, Angew. Chem. Int. Ed. 57 (2018) 8729–8733.
[58] C. Sun, H. Zhang, H. Liu, X. Zheng, W. Zou, L. Dong, L. Qi, Enhanced activity of visible-light photocatalytic H_2 evolution of sulfur-doped g-C_3N_4 photocatalyst via nanoparticle metal Ni as cocatalyst, Appl. Catal. B: Environ. 235 (2018) 66–74.
[59] H. Ou, L. Lin, Y. Zheng, P. Yang, Y. Fang, X. Wang, Tri-s-triazine-based crystalline carbon nitride nanosheets for an improved hydrogen evolution, Adv. Mater. 29 (2017) 1700008.
[60] N. Tian, Y. Zhang, X. Li, K. Xiao, X. Du, F. Dong, G.I.N. Waterhouse, T. Zhang, H. Huang, Precursor-reforming protocol to 3D mesoporous g-C_3N_4 established by ultrathin self-doped nanosheets for superior hydrogen evolution, Nano Energy 38 (2017) 72–81.
[61] M. Shalom, M. Guttentag, C. Fettkenhauer, S. Inal, D. Neher, A. Llobet, M. Antonietti, In situ formation of heterojunctions in modified graphitic carbon nitride: synthesis and noble metal free photocatalysis, Chem. Mater. 26 (2014) 5812–5818.
[62] Y. Huijun, S. Run, Z. Yunxuan, B. Tong, Z. Yufei, Z. Chao, G.I.N. Waterhouse, W. Li-Zhu, T. Chen-Ho, Z. Tierui, Alkali-assisted synthesis of nitrogen deficient graphitic carbon nitride with tunable band structures for efficient visible-light-driven hydrogen evolution, Adv. Mater. 29 (2017) 1605148.
[63] D.K.L. Chan, J.C. Yu, Facile synthesis of carbon- and oxygen-rich graphitic carbon nitride with enhanced visible-light photocatalytic activity, Catal. Today (2017).
[64] Z. Tong, D. Yang, Z. Li, Y. Nan, F. Ding, Y. Shen, Z. Jiang, Thylakoid-inspired multishell g-C_3N_4 nanocapsules with enhanced visible-light harvesting and electron transfer properties for high-efficiency photocatalysis, ACS Nano 11 (2017) 1103–1112.
[65] H. Wang, X. Sun, D. Li, X. Zhang, S. Chen, W. Shao, Y. Tian, Y. Xie, Boosting hot-electron generation: exciton dissociation at the order-disorder interfaces in polymeric photocatalysts, J. Am. Chem. Soc. 139 (2017) 2468–2473.
[66] C. Zhang, C. Lai, G. Zeng, D. Huang, C. Yang, Y. Wang, Y. Zhou, M. Cheng, Efficacy of carbonaceous nanocomposites for sorbing ionizable antibiotic sulfamethazine from aqueous solution, Water Res. 95 (2016) 103–112.
[67] M. Wu, T. Ding, J. Cai, Y. Wang, H. Xian, H. Zhang, Y. Tian, T. Zhang, X. Li, Coaddition of phosphorus and proton to graphitic carbon nitride for synergistically enhanced visible light photocatalytic degradation and hydrogen evolution, ACS Sustainable Chem. Eng. 6 (2018) 8167–8177.
[68] J. Zhang, X. Chen, K. Takanabe, K. Maeda, K. Domen, J.D. Epping, X. Fu, M. Antonietti, X. Wang, Synthesis of a carbon nitride structure for visible-light catalysis by copolymerization, Angew. Chem. Int. Ed. 49 (2010) 441–444.
[69] G. Dong, K. Zhao, L. Zhang, Carbon self-doping induced high electronic conductivity and photoreactivity of g-C_3N_4, Chem. Commun. (Cambridge) 48 (2012) 6178–6180.
[70] W. Xing, G. Chen, C. Li, Z. Han, Y. Hu, Q. Meng, Doping effect of non-metal group in porous ultrathin gC_3N_4 nanosheets towards synergistically improved photocatalytic hydrogen evolution, Nanoscale 10 (2018) 5239–5245.
[71] W. Wang, P. Xu, M. Chen, G. Zeng, C. Zhang, C. Zhou, Y. Yang, D. Huang, C. Lai, M. Cheng, L. Hu, W. Xiong, H. Guo, M. Zhou, Alkali metal-assisted synthesis of graphite carbon nitride with tunable band-gap for enhanced visible-light-driven photocatalytic performance, ACS Sustainable Chem. Eng. 6 (2018) 15503–15516.